Purinergic Signalling (2017) 13:61–74
DOI 10.1007/s11302-016-9539-y

ORIGINAL ARTICLE

2′,3′-*O*-Substituted ATP derivatives as potent antagonists of purinergic P2X3 receptors and potential analgesic agents

Diego Dal Ben[1] · Anna Marchenkova[2] · Ajiroghene Thomas[1] · Catia Lambertucci[1] · Andrea Spinaci[1] · Gabriella Marucci[1] · Andrea Nistri[2] · Rosaria Volpini[1]

Received: 22 April 2016 / Accepted: 19 September 2016 / Published online: 18 October 2016

Abstract Blocking membrane currents evoked by the activation of purinergic P2X3 receptors localized on nociceptive neurons represents a promising strategy for the development of agents useful for the treatment of chronic pain conditions. Among compounds endowed with such antagonistic action, 2′,3′-*O*-(2,4,6-trinitrophenyl)-ATP (TNP-ATP) is an ATP analogue, whose inhibitory activity on P2X receptors has been previously reported. Based on the results of molecular modelling studies performed with homology models of the P2X3 receptor, novel adenosine nucleotide analogues bearing cycloalkyl or arylalkyl substituents replacing the trinitrophenyl moiety of TNP-ATP were designed and synthesized. These new compounds were functionally evaluated on native P2X3 receptors from mouse trigeminal ganglion (TG) sensory neurons using patch clamp recordings under voltage clamp configuration. Our data show that some of these molecules are potent (nanomolar range) and reversible inhibitors of P2X3 receptors, without any apparent effect on trigeminal $GABA_A$ and 5-HT_3 receptors, whose membrane currents were unaffected by the tested compounds.

Keywords Purinergic receptors · P2X3 receptor antagonists · ATP derivatives · Purine derivatives · Patch clamp · Molecular modelling

Electronic supplementary material The online version of this article (doi:10.1007/s11302-016-9539-y) contains supplementary material, which is available to authorized users.

✉ Rosaria Volpini
rosaria.volpini@unicam.it

[1] School of Pharmacy, Medicinal Chemistry Unit, University of Camerino, via S. Agostino 1, 62032 Camerino, (MC), Italy

[2] Neuroscience Department, International School for Advanced Studies (SISSA), Via Bonomea 265, 34136 Trieste, Italy

Introduction

The nucleotide adenosine-5′-triphosphate (ATP, Fig. 1), which represents the main energy storage molecule in cells, is released from healthy or damaged tissues in high concentrations (mM range) and acts also as a neuromodulator interacting with specific membrane receptors belonging to the family of so-called purinergic P2 receptors. This receptor family comprises two different classes of membrane proteins named P2Y and P2X receptors, which are distinguished on the base of their structure and function. To date, eight subtypes of the P2Y receptors, belonging to the family of G protein coupled receptors (GPCRs), and seven subtypes (P2X1-7) of the P2X ion channels, permeable to Na^+, K^+, Ca^{++} ions and small molecules, have been cloned from humans [1–5]. P2X receptors assemble as homo- or heterotrimers [6, 7] and share a common structure, presenting intracellular N- and C-termini, two transmembrane domains (TM1 and TM2) and a large glycosylated and cysteine-rich extracellular domain [8–10]. When ATP binds to P2X receptors, a large conformational change causes the opening of the transmembrane pore allowing the cation flow and leading to the depolarization of the cell and generation of action potentials [11, 12]. After this activation process, the P2X1 and P2X3 receptor subtypes undergo rapid desensitization, while the P2X2, P2X4 and P2X7 subtypes desensitize slowly [13]. Since P2X receptor activity is involved in a number of physiological processes (regulation of cell cycle, muscle cell contraction, platelet aggregation, nociception and inflammation), they are considered as therapeutic targets for several conditions including cancer and inflammatory, neurological, cardiovascular and endocrine diseases [3, 5, 14–26].

The P2X3 receptors were cloned in 1995 [27, 28], and they are almost exclusively localized to nociceptive sensory ganglion neurons and nodose ganglion neurons [29, 30]. Different chronic pain diseases are linked to the upregulation of these

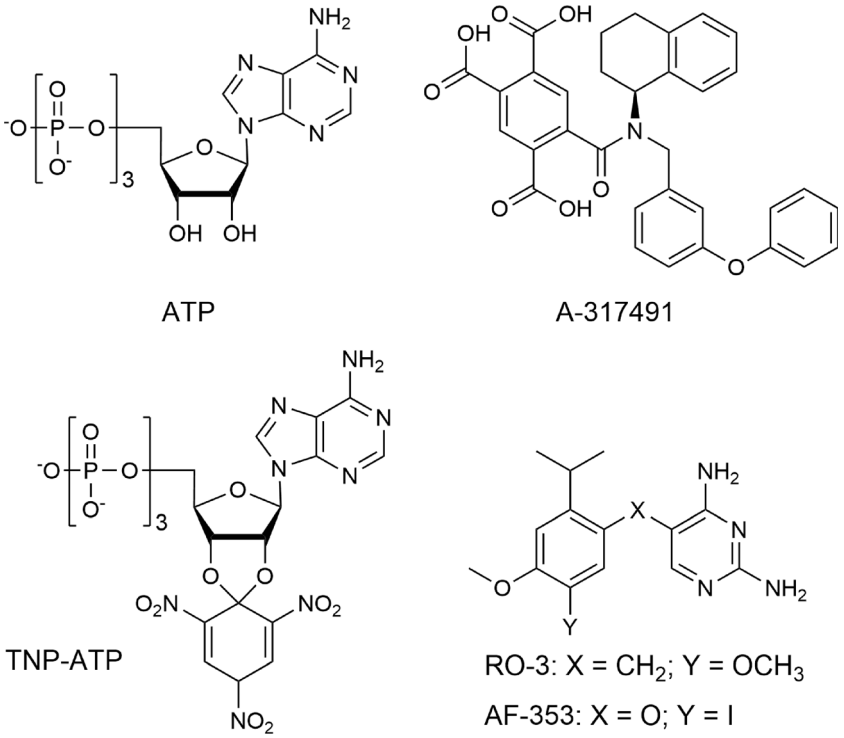

Fig. 1 Ligands of the P2X3 receptor

receptors (i.e. neuropathic and inflammatory pain, headache pain and migraine) [22, 31–39]. As a consequence, targeting these receptors represents an innovative therapeutic strategy to treat both neuropathic and inflammatory pain conditions [40, 41]. Recent papers described the rapid transition of the P2X3 receptors to a desensitization state followed by a relatively slow recovery of sensitivity to ATP [13, 42]. Hence, long-acting and low efficacy P2X3 agonists could be useful to block nociceptive transmission via receptor inactivation. Examples of such molecules are the so-called "acyclic nucleotides," which were obtained by modifying the sugar moiety of ATP [43].

Another approach to obtain analgesic agents acting on P2X3 receptors is by designing and synthesizing new antagonists. The first identified P2X3 antagonists were negatively charged and/or high molecular weight arylpolysulfonate molecules [44], which showed to be unselective, as they were able to antagonize also the metabotropic P2Y receptors [45]. Further studies led to the discovery of a potent and selective P2X3 receptor antagonist, named A-317491 (Fig. 1), showing nanomolar activity at both homomeric P2X3 and heteromeric P2X2/3 receptors [46]. The most potent competitive antagonist of P2X3 receptors is the 2′,3′-*O*-(2,4,6-trinitrophenyl)-ATP (TNP-ATP, Fig. 1) [47], with low nanomolar activity. In fact, this molecule showed to inhibit ATP or α,β-meATP evoked current at P2X3 receptors expressed by HEK293 cells with an IC_{50} value of 2 nM [48]. This molecule was also able to block (at 1 μM) by 91 % currents evoked by 100 μM α,β-meATP at rat TG neurons [49] and to block currents evoked by 30 μM α,β-meATP at mouse nodose neurons with an IC_{50} value of 11 nM [50]. Several P2X ligands were also discovered through high-throughput screening (HTS) studies which led to the discovery of a series of diaminopyrimidine derivatives, like RO-3 and AF-353 (Fig. 1), acting as allosteric P2X3 antagonists [51–53]. Substitution of the diaminopyrimidine scaffold with a diaminopurine moiety led to compounds that maintained the antagonistic behaviour [54].

The screening efforts represented for several years the only strategy to develop P2X ligands due to the lack of experimental structural data of P2X receptors. In 2009 and 2012, the crystal structures of the zebrafish P2X4 receptor (zP2X4) in the presence and absence of ATP were reported, providing structural details of these membrane proteins [55, 56], useful for the analysis of the ATP binding mode and the interpretation of mutagenesis data [12]. Furthermore, a comparative analysis of the open (active state) and closed (inactive state) receptor conformations provides a detailed view of the mechanism of P2X receptor activation.

We recently reported a molecular modelling analysis aimed at developing 3D models of the human and rat P2X receptors in both active and inactive state [57]. This study permitted the analysis of the binding mode of the agonist ATP and the antagonist TNP-ATP at the P2X3 receptor. The mechanism of TNP-ATP antagonism, proposed on the basis of its ability to prevent rearrangement of P2X subunits [56], was confirmed by P2X3 modelling studies [57]. The comparison of the binding mode of ATP and TNP-ATP led to an interpretation of the role of the 2′,3′-*O*-substituent in the antagonist molecule.

Starting from these results, we designed ATP analogues bearing different substituents in the 2′,3′-*O*-position as new P2X3 antagonists. In the present study, we report the design, synthesis and biological evaluation of three ATP derivatives presenting in the 2′,3′-*O*-position a cyclohexylidene or a benzylidene moiety. The design was made with the aid of molecular modelling using homology models of the human and mouse P2X3 receptors that share 93.7 % identical residues and have almost identical chemico-physical characteristics considering the respective ATP binding cavities. In the design phase, we decided to maintain the triphosphate chain of ATP even though it is known to have low chemical and metabolic stability [58]. Our choice was made in order to make the new molecules as similar as possible to the reference compound TNP-ATP and hence to evaluate the impact of the different 2′,3′-substituent on the compound potency. Furthermore, the corresponding monophosphate analogues of these compounds were also synthesized, since it was observed that the mono- or di-phosphate analogues of TNP-ATP were able to inhibit P2X3 receptors as well [48]. The compounds were evaluated for their biological activity on native P2X3 receptors of mouse TG sensory neurons, using patch clamp technique to record membrane currents. This method enabled a quantitative investigation of P2X3 agonist/antagonist interaction through the use of dose-response curves in the presence of the reference non-hydrolysable P2X3 agonist α,β-methyleneATP (α,β-meATP; P2X3 EC_{50} = 1.8 μM [59]). This approach also allowed us to study changes in receptor desensitization and to test if the new compounds were able to modify membrane currents evoked by activation of other membrane channels like 5-HT_3 or $GABA_A$ receptors that are expressed by TG neurons [60–63].

Results

Molecular modelling design

We already reported the TNP-ATP docking conformation at the inactive state human P2X3 binding site ([57] and Fig. 2). In summary, the compound presents a similar binding mode to the one of ATP, observable from X-ray data (zP2X4) and from ATP-bound homology models of human [57] and mouse (Supporting Material) P2X3 receptors developed using the zP2X4 X-ray structure in its active state (PDB code: 4DW1; 2.8-Å resolution [56]) as a template. The phosphate groups of the ligand are involved in a series of polar interactions with the binding cavity residues, most of them being positively charged residues (i.e. Lys63, Lys65, Ser275, Asn279, Arg281 and Lys299; Fig. 2). The adenine moiety is inserted between the side chains of Lys65, Phe174 and Ile215 and provides H-bonding with Thr172 backbone and side chain atoms. The 2′- and 3′-hydroxy groups of ATP are missing as the two oxygen atoms are bound to the trinitrophenyl function, which is inserted between two segments of adjacent P2X3 monomers and interacts with the residues located in its

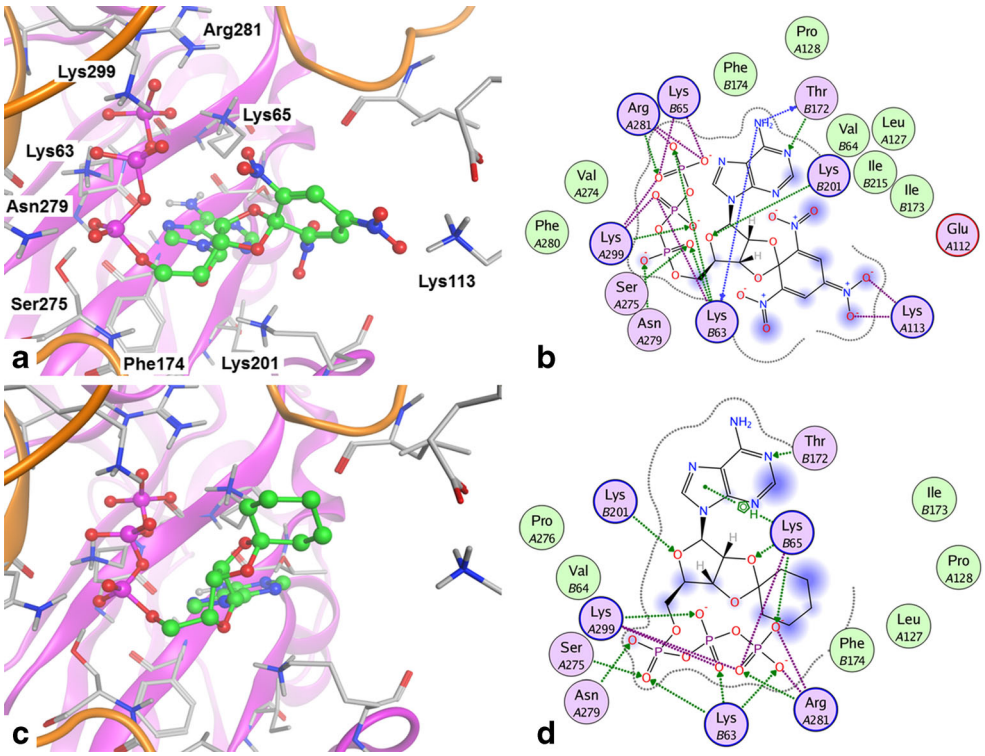

Fig. 2 **a**, **b** Docking conformation (schematic description in panel **b**) of TNP-ATP at the human P2X3 binding site. Main residues for the ligand-receptor interaction are indicated. **c**, **d** Design of new ligands; docking conformation of the compound **4** (schematic description in panel **d**)

proximity. At the same time, this group prevents the possible approach of the two monomers observed during the activation process of the receptor [56]. To verify that the role of the trinitrophenyl group is mainly related to its steric hindrance and not to other features given by its chemical structure (i.e. interaction given by the nitro groups), our design process was based on the substitution of the trinitrophenyl function with other groups presenting comparable volume even if with different chemical properties. Hence, we designed ATP derivatives bearing in the 2′,3′-*O*-position bulky groups like a cyclohexylidene or a benzylidene function (2′,3′-*O*-cyclohexylidene ATP and 2′,3′-*O*-benzylidene ATP, compounds **4**, **9** and **10**, respectively, see Schemes 1 and 2). The designed compounds were docked into the binding site of homology models of the human and mouse P2X3, built using the X-ray structure of the zP2X4 receptor in its apo (inactive) state (PDB code: 4DW0; 2.9-Å resolution [56]) as a template. Figure 2 reports a comparison of the simulated binding mode of the TNP-ATP and compound **4** at the human P2X3 binding site. In the Supporting Material, the binding mode of TNP-ATP and the new triphosphate derivatives at the mouse P2X3 plus the docking conformations of compounds **9** and **10** at the human and mouse receptors are reported. Docking results present compound **4** inserted into the binding cavity in a very similar way in respect to TNP-ATP, with the phosphate groups positioned close to the cluster of positively charged residues in the depth of the site. The adenine moiety is similarly positioned in respect to TNP-ATP (even if slightly reoriented when compared to the same group of the latter compound), while the cyclohexyl group is located within the interface of the two subunits in a similar way of the trinitrophenyl function of TNP-ATP. These data suggest that the new compound could provide a similar steric hindrance of the reference molecule and hence could behave as obstacle for the receptor activation mechanism in a similar way to TNP-ATP. Analogous results were observed for the triphosphate derivatives **9** and **10** (Supporting Material). The corresponding monophosphate analogues (compounds **3**, **7** and **8**, respectively) were synthesized as well, since it was observed that the mono- or di-phosphate derivatives of TNP-ATP were able to inhibit P2X3 receptors. In literature, we found that the compound **3** was already claimed in a patent describing nucleoside derivatives as P2X7 antagonists [64], although the synthesis and the biological activity of this compound were not reported. We also found that an analogue of the non-hydrolysable P2X ligand β,γ-meATP, bearing a 2′,3′-*O*-benzylidene substituent and hence similar to the compounds **9** and **10** presented in this work, was tested for its ability to induce contraction at rabbit ear central artery showing a micromolar activity at this tissue preparation [65].

Synthesis

New nucleotides **3** and **4** were prepared starting from the suitable nucleoside **2**. Reaction of commercially available adenosine (**1**) with freshly distilled cyclohexanone in the presence of *p*-toluenesulfonic acid and 4 Å molecular sieves (Scheme 1) yielded nucleoside **2** by using a modification of a previously reported procedure [64] in which this compound was not characterized. The purification of the reaction product by silica gel chromatography and crystallization from ethylacetate provided the intermediate compound **2** with 33 % yield.

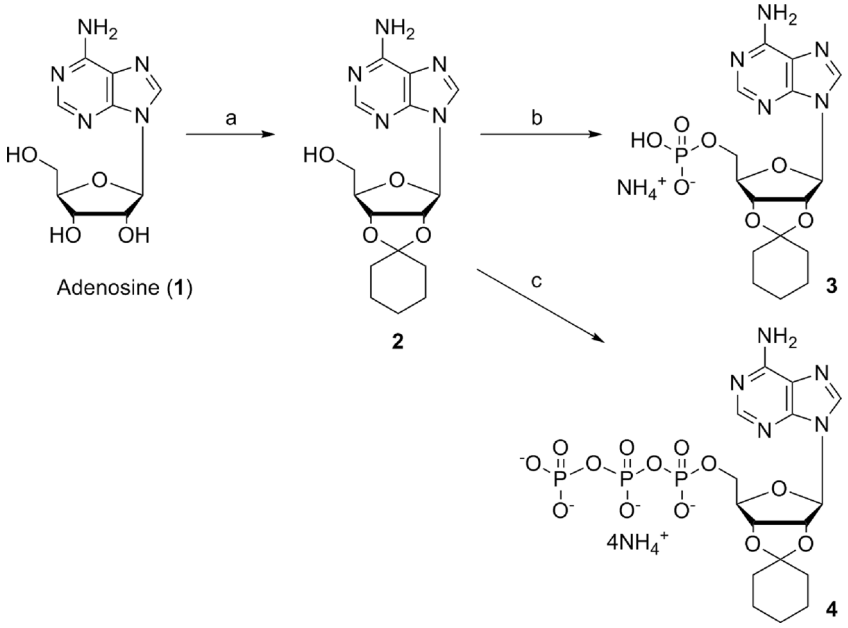

Scheme 1 Reagents and conditions: *a*, cyclohexanone, p-toluenesulfonic acid, 4 Å molecular sieves, 70 °C, 48 h; *b*, i. phosphorus oxychloride, dry trimethyl phosphate, 0 °C, 4 h; ii. 1 M TEAB, 0 °C to r. t., 15 min; *c*, i. phosphorus oxychloride, dry trimethyl phosphate, 0 °C, 4 h; ii. bis-(tri-*n*-butylammonium) pyrophosphate solution in dry DMF, 0 °C, 10 min; iii. 1 M TEAB, 0 °C to r. t., 15 min

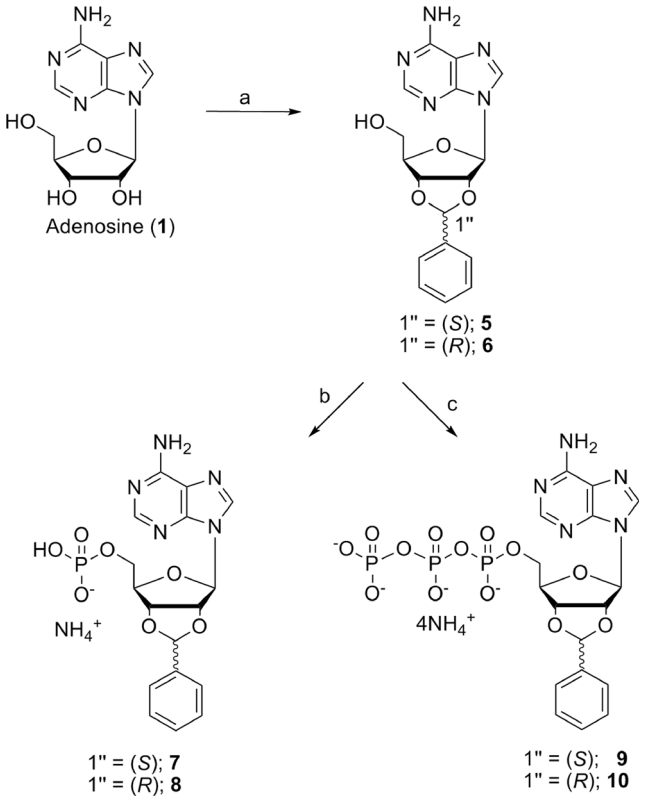

Scheme 2 Reagents and conditions: *a*, benzaldehyde, p-toluenesulfonic acid, 4 Å molecular sieves, 70 °C, 4 h. *b*, i. phosphorus oxychloride, dry trimethyl phosphate, 0 °C, 4 h; ii. 1 M TEAB, 0 °C to r. t., 15 min; *c*, i. phosphorus oxychloride, dry trimethyl phosphate, 0 °C, 4 h; ii. bis-(tri-*n*-butylammonium) pyrophosphate solution in dry DMF, 0 °C, 10 min; iii. 1 M TEAB, 0 °C to r. t., 15 min

On the other hand, the reaction of adenosine with benzaldehyde, using the same reaction conditions described before, supplied the suitable adenosine diastereomer derivatives **5** and **6** (Scheme 2). Although the synthesis of the 2′,3′-*O*-benzylidene adenosine was previously reported, the reaction was performed in different conditions with respect to this work and the single epimers obtained were not characterized [66]. Hence, these two epimers, compounds **5** and **6**, were separated by silica gel chromatography and characterized by NOESY-NMR experiments; in fact, irradiation of the ketal CH (H-1″ proton; Fig. 3) and measurements of its effects on the ribose protons allowed to unequivocally attribute the molecule configuration. By means of a 1D-NOESY experiment (Fig. 3), the irradiation of the signal at 6.02 ppm of compound **6**, corresponding to the ketal CH (1″ position), induced a signal increase of the peaks at 5.50, 5.08 and 7.56 corresponding to the H-2′and H-3′ protons of the sugar moiety and the hydrogens in the orto-position of the phenyl ring, respectively. Thus, we were able to ascribe the (*R*) configuration to the ketal position of the dioxolane ring of compound **6**, as the observed interactions between the ketal proton and the hydrogens at the 2′ and 3′ positions of the sugar moiety was possible only when the H-1″, H-2′ and H-3′ protons point toward the same side with respect to the ribose plane. In the case of compound **5**, a NOESY-2D NMR experiment was performed due to the close vicinity of the signals at 6.24 and 6.28 ppm, corresponding to the H-1″ and H-1′, respectively, which did not permit a selective irradiation of the ketal CH proton. In the obtained spectrum, a clear interaction between the protons at 6.24 (H-1″), 4.28 (H-4′) and at 7.50 (2H-Ph) ppm was observed.

The signal at 4.28 corresponds to the ketal CH (1″-position) of the dioxolane ring, while the other signals belong to the H-4′ of the sugar moiety and to the protons in the orto-position of the phenyl ring. In this case, we ascribed the (*S*) configuration to the ketal chiral centre of compound **5**. In fact, only when the H-1″ and the H-4′ protons are on the same side, it is possible to have proton magnetic field interaction.

The synthesis of desired nucleotides (compounds **3**, **7** and **8**) was performed by reaction of the suitable intermediates **2**, **5** and **6** with phosphorus oxychloride in trimethyl phosphate at 0 °C and subsequent quenching with a cold triethylammonium bicarbonate buffer solution. Compounds **3**, **7** and **8** were obtained as ammonium salts after ion exchange chromatography on a Sephadex DEAE resin eluted with a solvent gradient of 0

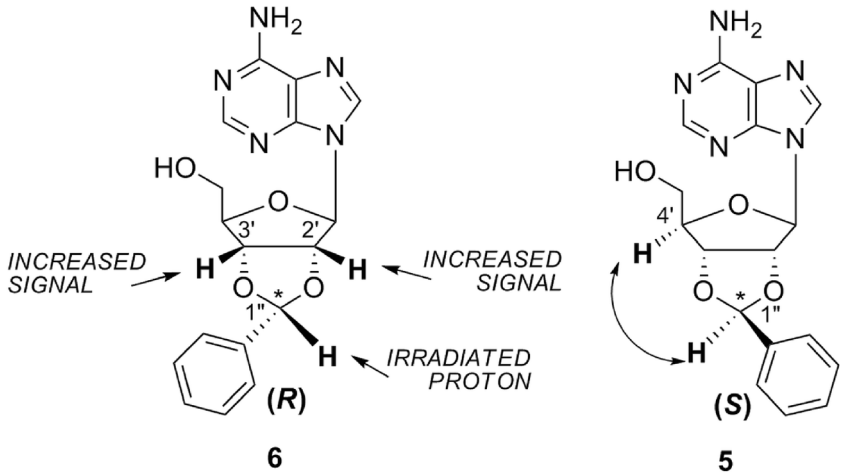

Fig. 3 NOESY-1D NMR characterization for the configuration assignment of epimers **6** and **5**

to 0.2 M ammonium bicarbonate buffer (Schemes 1 and 2). Previously, the diastereoisomeric mixture of **7** and **8** was obtained by reaction of adenosine monophosphate with the benzaldehyde dimethylacetal, without a full characterization of the separated diastereomers [67].

For the synthesis of the triphosphate derivatives **4**, **9** and **10**, after a first step reaction of the nucleosides **2**, **5** or **6** with phosphorus oxychloride in trimethylphosphate at 0 °C for 4 h, a bis(tri-*n*-butylammonium) pyrophosphate solution in dry DMF was added to the reaction mixtures. The reactions were then quenched by adding slowly a cold triethylammonium bicarbonate buffer solution and purified with ion exchange chromatography on a Sephadex DEAE resin eluting with a solvent gradient of 0 to 0.4 M ammonium bicarbonate buffer (Schemes 1 and 2). All nucleotides were characterized by ^{1}H-NMR and ^{31}P-NMR spectra, as usually performed.

Biological assays

Newly synthesized compounds **3**, **4** and **7**–**10** were tested for their biological activity at native mouse P2X3 receptors expressed by TG sensory neurons in culture by using the patch clamp recording technique as previously reported [37, 42, 43]. As a first approach, all compounds were applied for 5 min at 10 μM; none of them could elicit functional responses even at concentration of 10 μM, showing lack of agonist properties. However, as expected, they exhibited antagonistic activity on P2X3 receptors, since their application inhibited subsequent current responses evoked by 2 s pulses of 10 μM α,β-meATP (Fig. 4) [37, 42, 43]. Such inhibition was reversible, as the peak current amplitude fully or partially recovered after 5 min wash out. Hence, the most potent compounds were further evaluated also at lower concentrations up to 0.01 μM.

Table 1 shows the calculated percent inhibition of the mouse P2X3-mediated currents elicited by tested compounds. At the concentration of 10 μM, the monophosphate derivatives **3**, **7** and **8** showed no or low inhibition of P2X3 currents with a percent change of −0.9 ± 13 %, 27 ± 9 % and 44 ± 8 %, respectively. These compounds were, therefore, not tested at lower concentrations. The corresponding triphosphate derivatives **4**, **9** and **10** showed 100 % inhibition of the P2X3 currents at 10 μM concentration. Compounds **4** and **10** were able to produce an almost complete inhibition (99 %) even at 1 μM. At sub-micromolar level, compounds **4** and **10** elicited a dose-dependent inhibition (74 and 71 % at 0.5 μM, respectively), while compound **9** was less potent (34 % inhibition at the same concentration). Furthermore, compounds **4** and **10** behaved as moderate inhibitors also at nanomolar levels (30 and 43 % at 50 nM and 21 and 25 % at 10 nM concentrations, respectively). Hence, these compounds show high potency (although they are not efficacious as TNP-ATP, whose low nanomolar activity is described within the Introduction).

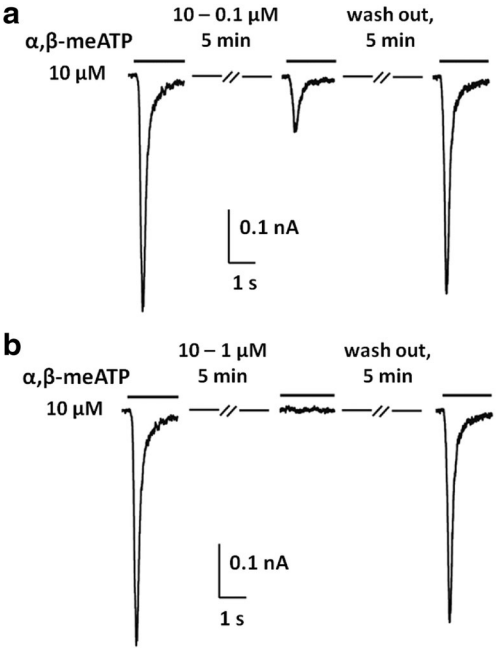

Fig. 4 Effect of the application of compound **10** on currents evoked by α,β-meATP at native mouse P2X3 receptors expressed by TG sensory neurons. The current evoked by 10 μM α,β-meATP was taken as control peak current and corresponds at a near-maximal response [37, 42]. After 5-min application of **10** (1 and 0.1 μM concentrations via fast superperfusion), subsequent application of 10 μM α,β-meATP induced smaller peak currents or no response at all. After 5-min washout, the current amplitude was almost completely restored. Figure 4 shows representative traces of the fast desensitizing inward currents evoked by 10 μM α,β-meATP and the effect of the synthesized compound **10** applied at 1 and 0.1 μM concentrations

Table 1 Summary of P2X3 antagonism of novel ATP derivatives

Compound	Concentration, μM	Inhibition of P2X3 current, %
3	10	−0.9 ± 13
7	10	27 ± 9
8	10	44 ± 8
4	0.01	21 ± 9
	0.05	30 ± 3
	0.1	74 ± 5
	1	99 ± 1
	10	100
10	0.01	25 ± 12
	0.05	43 ± 13
	0.1	71 ± 4
	1	99 ± 1
	10	100
9	0.01	7 ± 11
	0.05	18 ± 7
	0.1	34 ± 13
	1	86 ± 9
	10	100

Effects of the novel compounds were investigated on P2X3 currents evoked by 10 μM α,β-meATP; inhibition is expressed as % amplitude of control α,β-meATP-evoked current; data for each compound concentration are from 5 to 10 individual cells

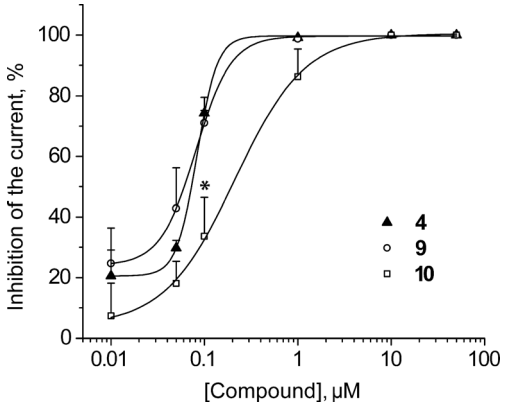

Fig. 5 Dose-inhibition curves of P2X3-mediated currents for compounds **4**, **9** and **10** built by applying different concentrations of antagonists using the same concentration of agonist (10 μM α,β-meATP). Data points from n = 5–10 cells, fitted with Hill equation (Eq. 2), *asterisk* indicates $p < 0.05$, two-sample t test

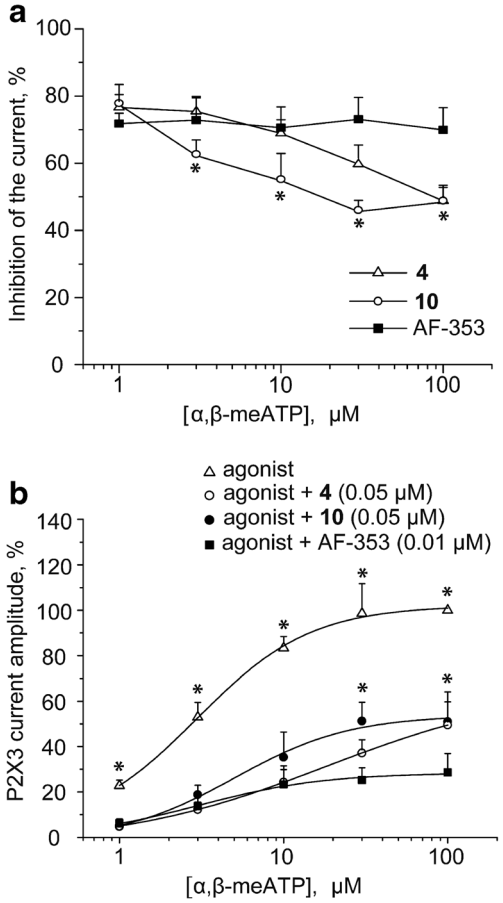

Fig. 6 Concentration-response curves for α,β-meATP-evoked P2X3 currents in control and with pre-application of compounds **4**, **10** and AF-353 (0.05 μM for **4** and **10**; 0.01 μM for AF-353). The agonist was applied at 1, 3, 10, 30 and 100 μM concentrations. Data for each point are obtained from 5 to 11 cells, *asterisk* indicates $p < 0.05$, two-sample t test

Dose response curves were built for the most potent compounds (**4**, **9** and **10**) as shown in Fig. 5, in which the log compound concentration was plotted against the percent inhibition of the α,β-meATP (10 μM) evoked current. Fitting the data with the Hill equation (Eq. 2; see experimental details) yielded for compound **4** a value of IC_{50} = 83 nM, for compound **10** a value of IC_{50} = 81 nM, and for compound **9** an IC_{50} = 211 nM (n = 5–10 cells). The difference of activity between the two isomers **9** and **10** is not particularly high (about 2.5-fold). Docking results show that the two compounds could share the binding mode to the receptor cavity and could give similar interaction with the protein residues. On the other hand, the arrangement of the *R*-isomer **10** appears more similar to the one of the reference compound TNP-ATP with respect to the *S*-isomer **9** (see Supporting Material Figure SI6). This data could explain the slightly higher potency of compound **10** compared to **9**. It is noteworthy that, as shown in Fig. 5, all three compounds produced full block of the agonist responses: these observations together with the absence of their direct stimulatory effect on P2X3 receptors (as reported earlier) confirm these novel compounds to be full antagonists.

To assess the mechanism of antagonism, we tested the ability of the two most potent compounds **4** and **10** to inhibit P2X3 currents evoked by different concentrations of the reference agonist α,β-meATP. The potent non-competitive P2X3 antagonist AF-353 [68] was also tested for comparison. These antagonists were tested at concentrations close to their IC_{50} values (0.05 μM for compounds **4** and **10**; 0.01 μM for AF-353) and applied for 5 min. The agonist α,β-meATP was applied for 2 s at 1, 3, 10, 30 and 100 μM concentrations. The dose-response curves are shown in Fig. 6. The extent of current inhibition evoked by AF-353 did not depend on the α,β-meATP concentration: this phenomenon is often referred to as non-competitive antagonism. Conversely, the inhibitory potency of compounds **4** and **10** appeared to decrease with increased agonist concentrations, suggesting a partially surmountable antagonism exerted by these two molecules when the agonist dose was raised (Fig. 6a). Figure 6b shows log agonist concentration/response plots in control solution or in the presence of each one of the three blockers. Since the curves were clearly shifted rightwards and downwards by compounds **4** or **10**, it appears that neither drug could induce competitive receptor antagonism that would have required preservation of the agonist maximum response and parallel shift of the dose response curve to the right. Thus, while the inhibition evoked by AF-353 could be minimally reversed by the P2X3 agonist, the antagonism by compounds **4** or **10** was partially surmounted by the higher agonist concentrations, suggesting a complex mode of pharmacological block in which the non-competitive antagonism process was predominant, yet not exclusive [69]. Nonetheless, in the presence of a competitive antagonist, receptors are prone to fast desensitization (that is strongly dependent on agonist concentration) and therefore might unexpectedly exhibit an apparent non-competitive antagonism when high agonist doses are used

and/or the antagonist facilitates the development of desensitization. In such cases, the agonist maximum effect would be decreased. We, therefore, explored if compounds **4** and **10** inhibited responses evoked by high agonist concentrations might be explained by facilitated receptor desensitization. If desensitization develops very rapidly, the response peak would be curtailed, thus summating desensitization-induced depression to any molecular antagonism by the novel compounds. Thus, we analysed P2X3 currents in control and after application of compound **10** with a two-exponential function [59] that allowed calculating the desensitization time constant τ_1 for both cases. Because τ_1 expresses the rate of current decay, it actually quantifies the speed at which the activated receptor enters into the desensitization state [59]. Since the desensitization constant τ_1 depends on the current amplitude that reflects the number of active receptors [59], to obtain suitable comparisons, the currents to be analysed should be approximately of the same size. Thus, we used lower agonist concentrations (5–10 μM) to elicit control currents and higher α,β-meATP concentration (30 μM) after application of compound **10** (0.03 μM), so that the evoked responses have comparable amplitudes. Figure 7 shows representative examples of superimposed current traces in control and after compound **10** (0.03 μM), recorded from the same cell.

As seen from the bar graph of Fig. 7, mean τ_1 values were not significantly different between the experimental conditions ($p = 0.41681$, paired t test), implicating that compound **10** did not affect the rate of agonist-induced desensitization.

P2X3 expressing sensory neurons such as DRG and TG are also known to express ionotropic 5-HT_3 and $GABA_A$ receptors [60–63]. We used this property to evaluate the receptor selectivity of the newly synthesized antagonists. As expected, the majority of TG neurons responded to GABA (93 %) and 5-HT (63 %) applied at 10 μM concentration. All these responses had fast rise-time (5-HT: τ_{on} = 65 ± 9 ms, n = 7; GABA: τ_{on} = 107 ± 9 ms, n = 10) and decay (5-HT: τ_{des1} = 145 ± 13 ms, τ_{des2} = 1.44 ± 0.28 s, n = 7; GABA: τ_{des} = 1.96 ± 0.39 s, n = 10) indicating that they were mediated by ionotropic receptors (5-HT_3 and $GABA_A$ receptors, respectively). Pre-application of 10 μM **4**, **9** or **10** did not significantly affected $GABA_A$ and 5-HT_3 currents, indicating that these compounds are selective for the P2X versus GABA and 5-HT receptors at TG neurons (Figure 8).

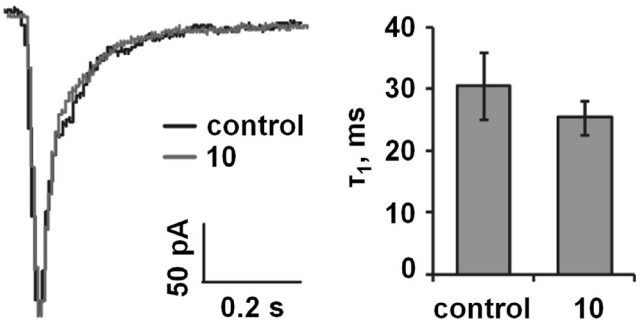

Fig. 7 Desensitization of P2X3 currents after application of compound **10**. Superimposed current traces from the same cell in control and after compound **10** (0.03 μM, 3 min) demonstrate no significant change in current decay time. Control current is induced by 10 μM α,β-meATP, current response after **10** treatment is evoked by 30 μM α,β-meATP. Histograms on the *right* show values of desensitization time constant τ_1 (mean ± S.E.); n cells = 7, p = 0.41681, paired t test

Conclusion

The principal finding of the present investigation is the demonstration of the highly potent and selective antagonism by newly synthesized compounds on P2X3 receptors of trigeminal sensory neurons. Since these receptors are strongly expressed by the vast majority of nociceptors in the trigeminal ganglion without concomitant expression of other P2X receptors [70, 71], this test system offers an advantageous opportunity to explore new antagonists and their potential value in dealing with trigeminal pain, an issue to be further studied with in vivo preclinical experiments. Thus, this work represents a starting point for a structure-based design of P2X3 antagonists as a strategy for the development of novel

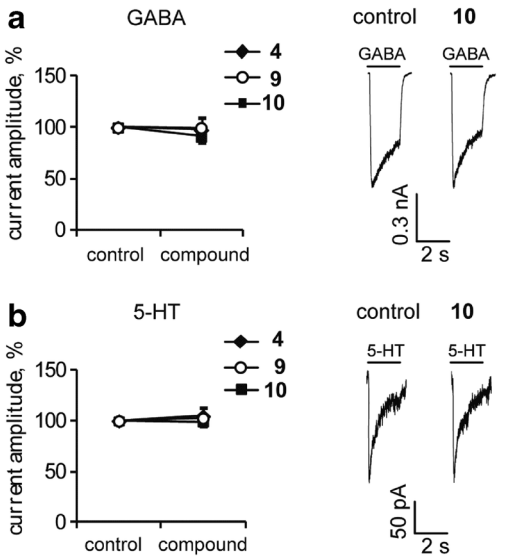

Fig. 8 Effect of compounds **4**, **9** and **10** on $GABA_A$ and 5-HT receptors. **a** Diagram on the *left* summarizes mean normalized peak amplitude values for currents evoked by 10 μM GABA (2 s pulses) in control and after 5-min application of compounds **4**, **10** or **9** (10 μM); n = 4, 6 and 5 for compounds **4**, **10** and **9**, respectively. Representative traces on the right show GABA-mediated currents in control and after treatment with compound **10**, recorded from the same cell. **b** Diagram on the *left* shows mean normalized peak amplitudes for currents evoked by 10 μM 5-HT (2 s pulses) in control and after 5-min application of compounds **4**, **10** or **9** (10 μM); n = 4. Examples of 5-HT-mediated current traces (recorded from a single cell) in control and after compound **10** application are presented on the right. $p > 0.05$ for each compound/receptor type, paired t test

potential analgesic drugs. The rationale was the hypothesis that the introduction of a bulky substituent in the 2′,3′-*O*-position of ATP, originally occupied by a 2,4,6-trinitrophenyl moiety in TNP-ATP, may confer antagonist activity of the obtained ATP derivatives at the P2X3 receptors. Hence, on the basis of molecular modelling studies, we designed and synthesized different mono- and triphosphate adenine nucleotides as TNP-ATP analogues in which the 2,4,6-trinitrophenyl function was replaced with cycloalkyl or arylalkyl groups. Patch-clamp recording experiments, performed on mouse P2X3 receptors expressed by TG sensory neurons, confirmed the original hypothesis demonstrating that the new triphosphate derivatives behave as potent P2X3 receptor antagonists, with IC_{50} in the nanomolar to submicromolar range. The antagonisms of these new nucleotides were selective at P2X3 receptors versus $GABA_A$ and 5-HT_3 receptors of the sensory TG neurons.

The future developments of the present work should deal with two key points. First, it can be expected that, as triphosphate derivatives, the synthesized compounds **4**, **9** and **10** might present low water and metabolic stability in physiological condition, i.e. when analysed in vivo. Hence, further optimization of these compounds should improve the chemical stability of the triphosphate chain. Second, the selectivity of the synthesized derivatives versus the other P2X receptor subtypes (not expressed by trigeminal neurons) will have to be determined, to verify if systemic administration of these compounds as analgesics might not be associated with pharmacological effects due to the activity on other members of the P2X receptor family expressed in distinct body tissues.

Experimental section

Molecular modelling

All molecular modelling studies were performed on a Core i7 CPU (PIV 2.20 GHZ) PC workstation. Homology modelling, energy minimization and docking studies were carried out using Molecular Operating Environment (MOE, version 2012.10) suite [72]. All ligand structures were optimized using RHF/AM1 semiempirical calculations and the software package MOPAC [73] implemented in MOE was utilized for these calculations.

Homology modelling of the human and mouse P2X3 receptor

Homology models of the human and mouse P2X3 receptor were built using the X-ray structure of the zP2X4 receptor in its apo (inactive) and ATP-bound (active) states (PDB code: 4DW0; 2.9-Å resolution and PDB code: 4DW1; 2.9-Å resolution as templates [56], respectively). A multiple alignment of the P2X receptor primary sequences was built within MOE as a preliminary step. The alignment of the sequences of human and mouse P2X3 and zP2X4 can be found within the Supporting Material. The boundaries identified from the used X-ray crystal structure of zP2X4 receptor were applied for the sequences of the human and mouse P2X3 receptors. The missing domains were built by the loop search method implemented in MOE. Once the heavy atoms were modelled, all hydrogen atoms were added and the protein coordinates were then minimized with MOE using the AMBER99 force field [74] until the root mean square (RMS) gradient of the potential energy was less than 0.05 kJ mol^{-1} $Å^{-1}$. Reliability and quality of the model were checked using the Protein Geometry Monitor application within MOE, which provides a variety of stereochemical measurements for inspection of the structural quality in a given protein, like backbone bond lengths, angles and dihedrals, Ramachandran φ-ψ dihedral plots, and sidechain rotamer and non-bonded contact quality.

Molecular docking analysis

The compound structures were docked into the binding site of the P2X3 receptor models using the MOE Dock tool. This method is divided into a number of stages. *Conformational Analysis of ligands*: The algorithm generated conformations from a single 3D conformation by conducting a systematic search. In this way, all combinations of angles were created for each ligand. *Placement*: A collection of poses was generated from the pool of ligand conformations using Triangle Matcher placement method. Poses were generated by superposition of ligand atom triplets and triplet points in the receptor binding site. The receptor site points are alpha sphere centres which represent locations of tight packing. At each iteration, a random conformation was selected, a random triplet of ligand atoms and a random triplet of alpha sphere centres were used to determine the pose. *Scoring*: Poses generated by the placement methodology were scored using two available methods implemented in MOE, the *London dG* scoring function which estimates the free energy of binding of the ligand from a given pose, and *Affinity dG* scoring which estimates the enthalpy contribution to the free energy of binding. The top 30 poses for each ligand were outputted to a MOE database.

Post docking analysis

The docking poses of each compound were then subjected to AMBER99 force field energy minimization until the RMS gradient of the potential energy was less than 0.05 kJ mol^{-1} $Å^{-1}$. Receptor residues within 6 Å distance from the ligand were left free to move, while the remaining receptor coordinates were kept fixed. AMBER99 partial charges of receptor and MOPAC output partial charges of ligands were utilized. Once the compound-binding site energy minimization was completed, receptor coordinates were fixed and a

second energy minimization stage was performed, leaving only compound atoms free to move. MMFF94 force field [75–81] was applied. For each compound, the minimized docking poses were then rescored using *London dG* and *Affinity dG* scoring functions and the *dock-pK_i* predictor. The latter tool allows estimating the pK_i for each ligand using the "scoring.svl" script retrievable at the SVL exchange service (Chemical Computing Group, Inc. SVL exchange: http://svl.chemcomp.com). The algorithm is based on an empirical scoring function consisting of a directional hydrogen-bonding term, a directional hydrophobic interaction term and an entropic term (ligand rotatable bonds immobilized in binding). The obtained pK_i values must be considered as docking scores and not as a prediction of binding affinity. For each compound, the three top-score docking poses according to at least two out of three scoring functions were selected for final ligand-target interaction analysis.

Chemistry

Melting points were determined with a Büchi apparatus and were uncorrected. ^{1}H-NMR and ^{31}P-NMR spectra were obtained with Varian Mercury 400 MHz spectrometer; δ in ppm, J in Hz; all exchangeable protons were confirmed by addition of D_2O. Mass spectra were recorded on an HP 1100-MSD series instrument. All measurements were performed using electrospray ionization (ESI-MS) on a single quadrupole analyser. TLC were carried out on pre-coated TLC plates with silica gel 60 F-254 (Merck). For column chromatography, silica gel 60 (Merck) was used. For ion exchange chromatography, Sephadex DEAE A-25 resin, HCO_3^- form, was used. Elemental analyses were determined on a Fisons model EA 1108 CHNS-O model analyser and are within ±0.4 % of theoretical values.

2′,3′-*O*-Cyclohexylideneadenosine (2) Adenosine (**1**, 3 g, 11.23 mmol) and *p*-toluenesulfonic acid (2.564 g, 13.48 mmol) were stirred at 70 °C in freshly distilled cyclohexanone (30 mL) in the presence of 4 Å molecular sieves. The reaction was stirred for 48 h, cooled to room temperature, neutralized with triethylamine, and the molecular sieves were filtered. Water (100 mL) was added and cyclohexanone was extracted with *n*-hexane (70 mL). The product was then extracted from the water phase with ethylacetate (100 mL × 4), dried over anhydrous Na_2SO_4 and evaporated to dryness. The residue was purified by silica gel flash column chromatography eluting with a gradient of 0 to 1.5 % MeOH in CH_2Cl_2 to give **2** (1.29 g, 3.70 mmol) with 33 % yield as a white powder after recrystallization from ethylacetate. M. p.: 173–175 °C; ^{1}H-NMR (DMSO-d_6, 400 MHz) δ 1.35 (m, 2H, *c*-Hex), 1.47 (m, 2H, *c*-Hex), 1.57 (m, 4H, *c*-Hex), 1.76 (m, 2H, *c*-Hex), 3.52 (m, 2H, H-5′), 4.20 (m, 1H, H-4′), 4.95 (dd, J = 2.0 Hz, J = 6.0 Hz, 1H, H-3′), 5.23 (t, J = 5.2 Hz, 1H, OH), 5.34 (dd, J = 2.8 Hz, J = 6.0 Hz, 1H, H-2′), 6.11 (d, J = 3.2 Hz, 1H, H-1′), 7.36 (s, 2H, NH_2), 8.14 (s, 1H, H-8), 8.33 ppm (s, 1H, H-2). ESI-MS: positive mode *m/z* 348.0 $[M + H]^+$, 370.0 $[M + Na]^+$, 717.0 $[2\ M + Na]^+$; negative mode *m/z* 346.2 $[M-H]^-$, 382.1 $[M + Cl]^-$. Anal. Calcd. for $C_{16}H_{21}N_5O_4$: C, 55.32; H, 6.09; N, 20.16; found: C, 55.39; H, 6.12; N, 20.11.

2′,3′-*O*-(*S*)-Benzylideneadenosine (5) and 2′,3′-*O*-(*R*)-benzylideneadenosine (6) Adenosine (**1**, 3 g, 11.23 mmol) and *p*-toluenesulfonic acid (2.564 g, 13.48 mmol) were stirred at 70 °C in freshly distilled benzaldehyde (53 mL) in the presence of 4 Å molecular sieves. The reaction was stirred for 4 h, cooled to room temperature, neutralized with triethylamine and the molecular sieves were filtered. One hundred millilitre of water was added and benzaldehyde was extracted with *n*-hexane (70 mL). The product was then extracted from the water phase with ethylacetate (100 mL × 4), dried over anhydrous Na_2SO_4 and evaporated to dryness. The residue was purified by silica gel normal column chromatography eluting with 4 % MeOH in CH_2Cl_2 to give **5** (672 mg, 1.89 mmol), 17 % yield, and **6** (1.484 g, 4.18 mmol), 37 % yield, as a white powders after recrystallization from ethylacetate. The configuration of the epimers was assigned based on NOESY-NMR experiment data.

5: m. p.: 217–219 °C; ^{1}H-NMR (DMSO-d_6, 400 MHz) δ 3.60 (m, 2H, H-5′), 4.28 (m, 1H, H-4′), 5.08 (m, 1H, H-3′), 5.17 (m, 1H, OH), 5.48 (m, 1H, H-2′), 6.24 (s, 1H, CH), 6.28 (d, J = 3.2 Hz, 1H, H-1′), 7.36 (s, 2H, NH_2), 7.43 (m, 3H, Ph), 7.50 (m, 2H, Ph), 8.15 (br s, 1H, H-8), 8.37 ppm (s, 1H, H-2). ESI-MS: positive mode *m/z* 355.9, 377.9, 732.9; negative mode *m/z* 354.1, 390.0. Anal. Calcd. for $C_{17}H_{17}N_5O_4$: C, 57.46; H, 4.82; N, 19.71; found: C, 57.51; H, 4.89; N, 19.67.

6: m. p.: 229–231 °C ; ^{1}H-NMR (DMSO-d_6, 400 MHz) δ 3.54 (m, 2H, H-5′), 4.36 (m, 1H, H-4′), 5.08 (dd, J = 2.4 Hz, J = 2.4 Hz, 1H, H-3′), 5.27 (t, J = 5.2 Hz, 1H, OH), 5.50 (dd, J = 2.4 Hz, J = 2.4 Hz, 1H, H-2′), 6.02 (s, 1H, CH), 6.28 (d, J = 2.8 Hz, 1H, H-1′), 7.37 (br s, 2H, NH_2), 7.46 (m, 3H, Ph), 7.56 (m, 2H, Ph), 8.15 (s, 1H, H-8), 8.37 ppm (s, 1H, H-2). ESI-MS: positive mode *m/z* 356.0, 377.9, 732.9; negative mode *m/z* 354.1. Anal. Calcd. for $C_{17}H_{17}N_5O_4$: C, 57.46; H, 4.82; N, 19.71; found: C, 57.49; H, 4.85; N, 19.64.

General procedure for the synthesis of monophosphates **3**, **7** *and* **8**

$POCl_3$ (52 μL, 0.56 mmol) was added dropwise in turn to a solution of **2**, **5** or **6** (50 mg, 0.14 mmol) in dry trimethylphosphate (0.7 mL) placed in an ice bath. The reaction was left to stir for 4 h, quenched by slowly adding 3 mL of a cold 1 M TEAB solution in an ice bath and then stirred for 15 min at r. t. The reaction mixtures were evaporated to dryness and co-evaporated with H_2O (3 × 5 mL). The obtained crude was purified over a Sephadex DEAE A-25 gel (HCO_3^- form) eluting with a solvent gradient of 0 to 0.2 M NH_4HCO_3

buffer. The appropriate fractions were collected, concentrated under vacuum and co-evaporated several times with H_2O to yield pure monophosphates **3**, **7** and **8** as white solids.

Adenosine-2′,3′-cyclohexylidene-5′-monophosphate ketal ammonium salt (3) The title compound was obtained from **2** with 93 % yield; ^{1}H-NMR (D_2O, 400 MHz) δ 1.26 (m, 2H, *c*-Hex), 1.38 (m, 2H, *c*-Hex), 1.52 (m, 4H, *c*-Hex), 1.73 (m, 2H, *c*-Hex), 3.87 (m, 2H, H-5′), 4.47 (m, 1H, H-4′), 5.00 (dd, J = 2.0 Hz, J = 2.0 Hz, 1H, H-3′), 5.23 (dd, J = 3.6 Hz, J = 3.6 Hz, 1H, H-2′), 6.09 (d, J = 3.6 Hz, 1H, H-1′), 8.05 (s, 1H, H-8), 8.24 ppm (s, 1H, H-2). ^{31}P-NMR (D_2O, 162 MHz) δ 1.69 ppm. ESI-MS: negative mode *m/z* 426.0, 853.2 Anal. Calcd. for $C_{16}H_{25}N_6O_7P$: C, 43.25; H, 5.67; N, 18.91; found: C, 43.31; H, 5.77; N, 18.88.

2′,3′-*O*-(*S*)-Benzylideneadenosine-5′-monophosphate ammonium salt (7) The title compound was obtained from **5** with 63 % yield; ^{1}H-NMR (D_2O, 400 MHz) δ 3.94 (m, 2H, H-5′), 4.46 (m, 1H, H-4′), 5.08 (dd, J = 3.6 Hz, J = 4.0 Hz, 1H, H-3′), 5.33 (dd, J = 2.8 Hz, J = 3.2 Hz, 1H, H-2′), 6.08 (s, 1H, CH), 6.17 (d, J = 3.6 Hz, 1H, H-1′), 7.29 (m, 3H, Ph), 7.36 (m, 2H, Ph), 8.01 (s, 1H, H-8), 8.18 ppm (s, 1H, H-2). ^{31}P-NMR (D_2O, 162 MHz) δ 1.25 ppm. ESI-MS: negative mode *m/z* 433.9, 869.0. Anal. Calcd. for $C_{17}H_{21}N_6O_7P$: C, 45.14; H, 4.68; N, 18.58; found: C, 45.23; H, 4.72; N, 18.55.

2′,3′-*O*-(*R*)-Benzylideneadenosine-5′-monophosphate ammonium salt (8) The title compound was obtained from **6** with 23 % yield; ^{1}H-NMR (D_2O, 400 MHz) δ 3.94 (m, 2H, H-5′), 4.63 (m, 1H, H-4′), 5.12 (dd, J = 1.6 Hz, J = 1.6 Hz, 1H, H-3′), 5.42 (dd, J = 2.8 Hz, J = 2.8 Hz, 1H, H-2′), 5.98 (s, 1H, CH), 6.31 (d, J = 2.4 Hz, 1H, H-1′), 7.38 (m, 3H, Ph), 7.52 (m, 2H, Ph), 8.12 (s, 1H, H-8), 8.32 ppm (s, 1H, H-2). ^{31}P-NMR (D_2O, 162 MHz) δ 0.98 ppm. ESI-MS: negative mode *m/z* 434.1. Anal. Calcd. for $C_{17}H_{21}N_6O_7P$: C, 45.14; H, 4.68; N, 18.58; found: C, 45.20; H, 4.75; N, 18.45.

General procedure for the synthesis of triphosphates **4**, **9** *and* **10**

$POCl_3$ (108 μL, 1.16 mmol) was added dropwise to a solution of **2**, **5**, or **6** (100 mg, 0.29 mmol) in dry trimethylphosphate (1.5 mL) placed in an ice bath. The reaction was left to stir for 4 h, after which 5.8 mL (2.90 mmol) of bis-(tri-*n*-butylammonium) pyrophosphate solution in dry DMF was added and stirred for 10 min. The reaction was quenched by slowly adding 5 mL of a cold 1 M TEAB solution in an ice bath and then stirred for 15 min at r. t. The mixture was extracted with *tert*-butylmethyl ether (3 × 15 mL), and the aqueous solution was evaporated and co-evaporated with H_2O (3 × 10 mL) to yield glassy oils. The obtained crude was purified over a Sephadex DEAE A-25 gel (HCO_3^- form) eluting with a solvent gradient of 0 to 0.4 M NH_4HCO_3 buffer. The appropriate fractions were collected, concentrated under vacuum, co-evaporated several times with H_2O to yield pure triphosphate derivatives **4**, **9** and **10** as white powders.

Adenosine-2′,3′-cyclohexylidene-5′-triphosphate ketal ammonium salt (4) The title compound was obtained from **2** with 25 % yield; ^{1}H-NMR (D_2O, 400 MHz) δ 1.29 (m, 2H, *c*-Hex), 1.40 (m, 2H, *c*-Hex), 1.56 (m, 4H, *c*-Hex), 1.77 (m, 2H, *c*-Hex), 4.05 (m, 2H, H-5′), 4.55 (m, 1H, H-4′), 5.09 (m, 1H, H-3′), 5.27 (dd, J = 3.2 Hz, J = 3.6 Hz, 1H, H-2′), 6.13 (d, J = 3.6 Hz, 1H, H-1′), 8.11 (s, 1H, H-8), 8.32 ppm (s, 1H, H-2). ^{31}P-NMR (D_2O, 162 MHz) δ − 9.63, −10.65, −22.06 ppm. ESI-MS: negative mode *m/z* 292.5, 586.1. Anal. Calcd. for $C_{16}H_{36}N_9O_{13}P_3$: C, 29.32; H, 5.54; N, 19.23; found: C, 29.38; H, 5.61; N, 19.18.

2′,3′-*O*-(*S*)-Benzylideneadenosine-5′-triphosphate ammonium salt (9) The title compound was obtained from **5** with 29 % yield; ^{1}H-NMR (D_2O, 400 MHz) δ 4.14 (m, 2H, H-5′), 4.65 (m, 1H, H-4′), 5.22 (m, 1H, H-3′), 5.42 (dd, J = 3.6 Hz, J = 3.6 Hz, 1H, H-2′), 6.21 (s, 1H, CH), 6.29 (d, J = 4.0 Hz, 1H, H-1′), 7.37 (m, 3H, Ph), 7.47 (m, 2H, Ph), 8.12 (s, 1H, H-8), 8.31 ppm (s, 1H, H-2). ^{31}P-NMR (D_2O, 162 MHz) δ − 9.22, −10.53, −22.04 ppm. ESI-MS: negative mode *m/z* 296.5, 594.0. Anal. Calcd. for $C_{17}H_{32}N_9O_{13}P_3$: C, 30.78; H, 4.86; N, 19.00; found: C, 30.84; H, 4.95; N, 18.92.

2′,3′-*O*-(*R*)-Benzylideneadenosine-5′-triphosphate ammonium salt (10) The title compound was obtained from **6** with 39 % yield:. ^{1}H-NMR (D_2O, 400 MHz) δ 4.04 (m, 1H, *H*CH-5′), 4.10 (m, 1H, *H*CH − 5′), 4.65 (m, 1H, H-4′), 5.20 (m, 1H, H-3′), 5.40 (dd, J = 3.2 Hz, J = 3.2 Hz, 1H, H-2′), 6.00 (s, 1H, CH), 6.28 (d, J = 3.2 Hz, 1H, H-1′), 7.38 (m, 3H, Ph), 7.53 (m, 2H, Ph), 8.06 (s, 1H, H-8), 8.33 ppm (s, 1H, H-2). ^{31}P-NMR (D_2O, 162 MHz) δ − 9.14, −10.66, −21.92 ppm. ESI-MS: negative mode *m/z* 296.6, 593.9. Anal. Calcd. for $C_{17}H_{32}N_9O_{13}P_3$: C, 30.78; H, 4.86; N, 19.00; found: C, 30.84; H, 4.91; N, 18.96.

Biological assays

Trigeminal ganglia culture neurons

Cultures of TG sensory neurons were prepared from C57Bl/6 wild type mice (P10–14) as previously described [70]. In brief, TG were rapidly excised and enzymatically dissociated in F12 Medium (Invitrogen Corp, Milan, Italy) containing 0.25 mg/mL trypsin, 1 mg/mL collagenase, 0.2 mL DNAse (Sigma, Milan, Italy) at 37 °C for 12 min. Cells were plated on poly-L-lysine coated 35 mm Petri dishes on F12 medium supplemented with 10 % foetal bovine serum and antibiotics and incubated for 24 h (5 % CO_2/95 % humidity, 37 °C).

Patch clamp recordings

Currents were recorded from small/medium size mouse TG neurons (nociceptors that strongly express native P2X3 receptors [70]) as previously described [70, 82] in whole cell voltage clamp configuration, at a holding potential of −65 mV after correction for liquid junction potential. Cells were continuously superfused at room temperature with control solution containing (in mM): 152 NaCl, 5 KCl, 1 $MgCl_2$, 2 $CaCl_2$, 10 glucose, 10 HEPES; pH 7.4 adjusted with NaOH. Patch pipettes had a resistance of 3–4 MΩ when filled with following solution (in mM): 140 KCl, 2 $MgCl_2$, 0.5 $CaCl_2$, 2 ATP-Mg, 2 GTP-Li, 10 HEPES, 10 EGTA; pH 7.2 adjusted with KOH (for recordings from TG neurons). After obtaining whole cell configuration, cell slow capacitance was compensated. Access resistance was never >10 MΩ and was routinely compensated by at least 70 %. One kilohertz filtering was used during recording; currents were acquired by means of a DigiData 1200 interface and pClamp8.2 software (Molecular Devices, Sunnyvale, CA, USA).

Drug application and data analysis

The receptor agonist α,β-meATP (Sigma) and test compounds were applied by rapid solution changer system (Rapid Solution Changer RSC-200; BioLogic Science Instruments, Claix, France). Membrane currents were analysed in terms of their peak amplitude and rise time (10–90 % of the peak). Current decay due to receptor desensitization during agonist application was fitted with either a monoexponential or biexponential function using pCLAMP Clampfit 9.2. Test compounds were kept at +4 °C and dissolved to 10 mM in H_2O before experiments and finally diluted to necessary concentration in control solution. For routine tests, the P2X3 selective agonist α,β-meATP was applied at 10 μM concentration (2 s pulse) at least 3 times (at 5 min interval to prevent cumulative receptor desensitization) to obtain an average control response. Since activated P2X3 receptors desensitize rapidly in the sustained presence of agonist, the inward current transient is, of course, too short for the binding equilibrium to be reached when agonist and antagonist are co-applied. Thus, to assess potential receptor blocking activity, each test compound was continuously pre-applied for 5 min before the α,β-meATP application as previously reported [42, 43]. Antagonist activity was quantified as percent inhibition of the α,β-meATP-induced current:

$$\%\text{inhibition} = 100*(1-I_2/I_1), \quad (1)$$

where I_1 is the control peak current, I_2 is the peak amplitude of the current after test compound.

For the most potent compounds, antagonist dose-inhibition curves were constructed by applying for 5 min different concentrations of each test compound using the same maximal concentration (10 μM) of α,β-meATP agonist. Data were plotted and fitted with empirical Hill equation using Origin 6.0 (Microcal, Northampton, MA, USA):

$$\%\text{inhibition} = 100/\left(1+(IC_{50}/[\text{Ant}])^{nH}\right), \quad (2)$$

where [Ant] is the concentration of the antagonist, n_H is the Hill coefficient, IC_{50} is the concentration of antagonist required to block the maximal current by 50 %. Agonist concentration-response curves in terms of normalized currents versus log agonist concentration were fitted with the same Hill equation, with corresponding parameters EC_{50} and n_H, where EC_{50} is the concentration of agonist required to produce the half-maximal current. All data are presented as mean ± standard error of the mean (S.E.); *n* is the number of cells. Statistical significance was evaluated with paired Student's *t* test (for parametric data) or Mann–Whitney rank-sum test (for nonparametric data), as suggested by the software; $p < 0.05$ was considered statistically significant.

Acknowledgment This work was supported by Fondo di Ricerca di Ateneo (FPI000033 - University of Camerino) and the EU FP7 grant EuroHeadPain (#602633).

Compliance with Ethical Standards As the corresponding authors of the manuscript entitled "2′,3′-O-Substituted ATP derivatives as potent antagonists of purinergic P2X3 receptors and potential analgesic agents" I declare that:

All the authors have not any conflict of interest

Research involving Animals

All animal experiments were done in full accordance with the European Union guidelines for animal use and the experimental protocols were approved by the ethics committee of International School for Advanced Studies (SISSA).

Conflict of Interest The authors declare that they have no conflict of interest.

References

1. Burnstock G (2012) Discovery of purinergic signalling, the initial resistance and current explosion of interest. Br J Pharmacol 167: 238–255
2. Abbracchio MP, Burnstock G, Verkhratsky A, Zimmermann H (2009) Purinergic signalling in the nervous system: an overview. Trends Neurosci 32:19–29
3. Surprenant A, North RA (2009) Signaling at purinergic P2X receptors. Annu Rev Physiol 71:333–359
4. Burnstock G, Fredholm BB, North RA, Verkhratsky A (2010) The birth and postnatal development of purinergic signalling. Acta Physiol (Oxf) 199:93–147

5. Khakh BS, North RA (2006) P2X receptors as cell-surface ATP sensors in health and disease. Nature 442:527–532
6. Dal Ben D, Adinolfi E (2015) Editorial: purinergic P2X receptors: physiological and pathological roles and potential as therapeutic targets. Curr Med Chem 22:782
7. Dal Ben D, Adinolfi E (2015) Special issue: purinergic P2X receptors: physiological and pathological roles and potential as therapeutic targets. Curr Med Chem 22:782–941
8. Young MT (2010) P2X receptors: dawn of the post-structure era. Trends Biochem Sci 35:83–90
9. Browne LE, Jiang LH, North RA (2010) New structure enlivens interest in P2X receptors. Trends Pharmacol Sci 31:229–237
10. Evans RJ (2010) Structural interpretation of P2X receptor mutagenesis studies on drug action. Br J Pharmacol 161:961–971
11. Grimes L, Young MT (2015) Purinergic P2X receptors: structural and functional features depicted by X-ray and molecular modelling studies. Curr Med Chem 22:783–798
12. Hausmann R, Kless A, Schmalzing G (2015) Key sites for P2X receptor function and multimerization: overview of mutagenesis studies on a structural basis. Curr Med Chem 22:799–818
13. North RA (2002) Molecular physiology of P2X receptors. Physiol Rev 82:1013–1067
14. Burnstock G, Kennedy C (2011) P2X receptors in health and disease. Adv Pharmacol 61:333–372
15. Burnstock G (2008) Purinergic signalling and disorders of the central nervous system. Nat Rev Drug Discov 7:575–590
16. Coddou C, Yan Z, Obsil T, Huidobro-Toro JP, Stojilkovic SS (2011) Activation and regulation of purinergic P2X receptor channels. Pharmacol Rev 63:641–683
17. Ralevic V (2015) P2X receptors in the cardiovascular system and their potential as therapeutic targets in disease. Curr Med Chem 22: 851–865
18. Jorgensen NR, Syberg S, Ellegaard M (2015) The role of P2X receptors in bone biology. Curr Med Chem 22:902–914
19. Fotino C, Vergani A, Fiorina P, Pileggi A (2015) P2X receptors and diabetes. Curr Med Chem 22:891–901
20. Di Virgilio F (2015) P2X receptors and inflammation. Curr Med Chem 22:866–877
21. Burnstock G (2015) Physiopathological roles of P2X receptors in the central nervous system. Curr Med Chem 22:819–844
22. Bele T, Fabbretti E (2015) P2X receptors, sensory neurons and pain. Curr Med Chem 22:845–850
23. Adinolfi E, Capece M, Amoroso F, De Marchi E, Franceschini A (2015) Emerging roles of P2X receptors in cancer. Curr Med Chem 22:878–890
24. Muller CE (2015) Medicinal chemistry of P2X receptors: allosteric modulators. Curr Med Chem 22:929–941
25. Lambertucci C, Dal Ben D, Buccioni M, Marucci G, Thomas A, Volpini R (2015) Medicinal chemistry of P2X receptors: agonists and orthosteric antagonists. Curr Med Chem 22:915–928
26. Jacobson KA, Muller CE (2015) Medicinal chemistry of adenosine, P2Y and P2X receptors. Neuropharmacology. doi:10.1016/j.neuropharm.2015.12.001
27. Chen CC, Akopian AN, Sivilotti L, Colquhoun D, Burnstock G, Wood JN (1995) A P2X purinoceptor expressed by a subset of sensory neurons. Nature 377:428–431
28. Lewis C, Neidhart S, Holy C, North RA, Buell G, Surprenant A (1995) Coexpression of P2X2 and P2X3 receptor subunits can account for ATP-gated currents in sensory neurons. Nature 377:432–435
29. Bradbury EJ, Burnstock G, McMahon SB (1998) The expression of P2X3 purinoreceptors in sensory neurons: effects of axotomy and glial-derived neurotrophic factor. Mol Cell Neurosci 12:256–268
30. Dunn PM, Zhong Y, Burnstock G (2001) P2X receptors in peripheral neurons. Prog Neurobiol 65:107–134
31. Jarvis MF (2003) Contributions of P2X3 homomeric and heteromeric channels to acute and chronic pain. Expert Opin Ther Targets 7:513–522
32. Chizh BA, Illes P (2001) P2X receptors and nociception. Pharmacol Rev 53:553–568
33. Souslova V, Cesare P, Ding Y, Akopian AN, Stanfa L, Suzuki R, Carpenter K, Dickenson A, Boyce S, Hill R, Nebenuis-Oosthuizen D, Smith AJ, Kidd EJ, Wood JN (2000) Warm-coding deficits and aberrant inflammatory pain in mice lacking P2X3 receptors. Nature 407:1015–1017
34. Cockayne DA, Hamilton SG, Zhu QM, Dunn PM, Zhong Y, Novakovic S, Malmberg AB, Cain G, Berson A, Kassotakis L, Hedley L, Lachnit WG, Burnstock G, McMahon SB, Ford AP (2000) Urinary bladder hyporeflexia and reduced pain-related behaviour in P2X3-deficient mice. Nature 407:1011–1015
35. Bian X, Ren J, DeVries M, Schnegelsberg B, Cockayne DA, Ford AP, Galligan JJ (2003) Peristalsis is impaired in the small intestine of mice lacking the P2X3 subunit. J Physiol 551:309–322
36. Rae MG, Rowan EG, Kennedy C (1998) Pharmacological properties of P2X3-receptors present in neurones of the rat dorsal root ganglia. Br J Pharmacol 124:176–180
37. Fabbretti E, D'Arco M, Fabbro A, Simonetti M, Nistri A, Giniatullin R (2006) Delayed upregulation of ATP P2X3 receptors of trigeminal sensory neurons by calcitonin gene-related peptide. J Neurosci 26:6163–6171
38. Ford AP, Gever JR, Nunn PA, Zhong Y, Cefalu JS, Dillon MP, Cockayne DA (2006) Purinoceptors as therapeutic targets for lower urinary tract dysfunction. Br J Pharmacol 147(Suppl 2):S132–S143
39. Burnstock G (2011) Therapeutic potential of purinergic signalling for diseases of the urinary tract. BJU Int 107:192–204
40. Brederson JD, Jarvis MF (2008) Homomeric and heteromeric P2X3 receptors in peripheral sensory neurons. Curr Opin Investig Drugs 9:716–725
41. Wirkner K, Sperlagh B, Illes P (2007) $P2X_3$ receptor involvement in pain states. Mol Neurobiol 36:165–183
42. Sokolova E, Skorinkin A, Fabbretti E, Masten L, Nistri A, Giniatullin R (2004) Agonist-dependence of recovery from desensitization of $P2X_3$ receptors provides a novel and sensitive approach for their rapid up or downregulation. Br J Pharmacol 141: 1048–1058
43. Volpini R, Mishra RC, Kachare DD, Dal Ben D, Lambertucci C, Antonini I, Vittori S, Marucci G, Sokolova E, Nistri A, Cristalli G (2009) Adenine-based acyclic nucleotides as novel $P2X_3$ receptor ligands. J Med Chem 52:4596–4603
44. Brown SG, Kim Y-C, Kim S-A, Jacobson KA, Burnstock G, F KB (2001) Actions of a series of PPADS analogs at P2X1 and P2X3 receptors. Drug Dev Res 53:281–291
45. Brown C, Tanna B, Boarder MR (1995) PPADS: an antagonist at endothelial P2Y-purinoceptors but not P2U-purinoceptors. Br J Pharmacol 116:2413–2416
46. Jarvis MF, Burgard EC, McGaraughty S, Honore P, Lynch K, Brennan TJ, Subieta A, Van Biesen T, Cartmell J, Bianchi B, Niforatos W, Kage K, Yu H, Mikusa J, Wismer CT, Zhu CZ, Chu K, Lee CH, Stewart AO, Polakowski J, Cox BF, Kowaluk E, Williams M, Sullivan J, Faltynek C (2002) A-317491, a novel potent and selective non-nucleotide antagonist of P2X3 and P2X2/3 receptors, reduces chronic inflammatory and neuropathic pain in the rat. Proc Natl Acad Sci U S A 99:17179–17184
47. Burgard EC, Niforatos W, van Biesen T, Lynch KJ, Kage KL, Touma E, Kowaluk EA, Jarvis MF (2000) Competitive antagonism of recombinant $P2X_{2/3}$ receptors by 2', 3'-O-(2,4,6-trinitrophenyl) adenosine 5'-triphosphate (TNP-ATP. Mol Pharmacol 58:1502–1510
48. Virginio C, Robertson G, Surprenant A, North RA (1998) Trinitrophenyl-substituted nucleotides are potent antagonists

selective for P2X1, P2X3, and heteromeric P2X2/3 receptors. Mol Pharmacol 53(6):969–973
49. Li HY, Lee BK, Kim JS, Jung SJ, SB O (2008) Eugenol inhibits ATP-induced P2X currents in trigeminal ganglion neurons. Korean J Physiol Pharmacol 12(6):315–321. doi:10.4196/kjpp.2008.12.6.315
50. Zhong Y, Dunn PM, Bardini M, Ford AP, Cockayne DA, Burnstock G (2001) Changes in P2X receptor responses of sensory neurons from P2X3-deficient mice. Eur J Neurosci 14(11):1784–1792
51. Carter D, Dillon MP, Hawley RC, Lin CJJ, Parish DW, Broka CA, Jahangir A (2005) Diaminopyrimidines as $P2X_3$ and $P2X_{2/3}$ antagonists. WO2005095359.
52. Carter DS, Alam M, Cai H, Dillon MP, Ford AP, Gever JR, Jahangir A, Lin C, Moore AG, Wagner PJ, Zhai Y (2009) Identification and SAR of novel diaminopyrimidines. Part 1: the discovery of RO-4, a dual $P2X_3$/$P2X_{2/3}$ antagonist for the treatment of pain. Bioorg Med Chem Lett 19:1628–1631
53. Muller CE (2010) Emerging structures and ligands for $P2X_3$ and $P2X_4$ receptors-towards novel treatments of neuropathic pain. Purinergic Signal 6:145–148
54. Lambertucci C, Sundukova M, Kachare DD, Panmand DS, Dal Ben D, Buccioni M, Marucci G, Marchenkova A, Thomas A, Nistri A, Cristalli G, Volpini R (2013) Evaluation of adenine as scaffold for the development of novel P2X3 receptor antagonists. Eur J Med Chem 65:41–50
55. Kawate T, Michel JC, Birdsong WT, Gouaux E (2009) Crystal structure of the ATP-gated P2X4 ion channel in the closed state. Nature 460:592–598
56. Hattori M, Gouaux E (2012) Molecular mechanism of ATP binding and ion channel activation in P2X receptors. Nature 485:207–212
57. Dal Ben D, Buccioni M, Lambertucci C, Marucci G, Thomas A, Volpini R (2015) Purinergic P2X receptors: structural models and analysis of ligand-target interaction. Eur J Med Chem 89:561–580
58. D'Ambrosi N, Costanzi S, Angelini DF, Volpini R, Sancesario G, Cristalli G, Volonte C (2004) 2-ClATP exerts anti-tumoural actions not mediated by P2 receptors in neuronal and glial cell lines. Biochem Pharmacol 67(4):621–630
59. Sokolova E, Skorinkin A, Moiseev I, Agrachev A, Nistri A, Giniatullin R (2006) Experimental and modeling studies of desensitization of P2X3 receptors. Mol Pharmacol 70:373–382
60. Morales M, McCollum N, Kirkness EF (2001) 5-HT_3-receptor subunits A and B are co-expressed in neurons of the dorsal root ganglion. J Comp Neurol 438:163–172
61. Nicholson R, Small J, Dixon AK, Spanswick D, Lee K (2003) Serotonin receptor mRNA expression in rat dorsal root ganglion neurons. Neurosci Lett 337:119–122
62. Stoyanova II (2004) Gamma-aminobutiric acid immunostaining in trigeminal, nodose and spinal ganglia of the cat. Acta Histochem 106:309–314
63. Hu WP, You XH, Guan BC, Ru LQ, Chen JG, Li ZW (2004) Substance P potentiates 5-HT3 receptor-mediated current in rat trigeminal ganglion neurons. Neurosci Lett 365:147–152
64. Douglass JG, Shaver SR, Navratil T, Boyer JL, Samuelson CA, DeCamp JB (2010) Method for treating inflammatory conditions. WO2010080540A1.
65. Martin PL, Gero TW, Potts AA, Cusack NJ (1995) Structure-activity studies of analogs of β,γ-methylene-ATP at P2X-purinoceptors in the rabbit ear central artery. Drug Dev Res 36:153–165
66. Redwan IN, Ljungdahl T, Grøtli M (2012) Investigation, optimization and synthesis of sulfamoyloxy-linked aminoacyl-AMP analogues. Tetrahedron 68(5):1507–1514
67. Douglass JG, Patel RI, Yerxa BR, Shaver SR, Watson PS, Bednarski K, Plourde R, Redick CC, Brubaker K, Jones AC, Boyer JL (2008) Lipophilic modifications to dinucleoside polyphosphates and nucleotides that confer antagonist properties at the platelet P2Y12 receptor. J Med Chem 51(4):1007–1025
68. Gever JR, Soto R, Henningsen RA, Martin RS, Hackos DH, Panicker S, Rubas W, Oglesby IB, Dillon MP, Milla ME, Burnstock G, Ford AP (2010) AF-353, a novel, potent and orally bioavailable P2X3/P2X2/3 receptor antagonist. Br J Pharmacol 160(6):1387–1398
69. Kenakin T (1993) Pharmacologic analysis of drug-receptor interaction, 2nd edn. Raven Press, New York
70. Simonetti M, Fabbro A, D'Arco M, Zweyer M, Nistri A, Giniatullin R, Fabbretti E (2006) Comparison of P2X and TRPV1 receptors in ganglia or primary culture of trigeminal neurons and their modulation by NGF or serotonin. Mol Pain 2:11
71. Staikopoulos V, Sessle BJ, Furness JB, Jennings EA (2007) Localization of P2X2 and P2X3 receptors in rat trigeminal ganglion neurons. Neuroscience 144(1):208–216
72. Molecular Operating Environment. C.C.G., Inc., 1255 University St., Suite 1600, Montreal, Quebec, Canada, H3B 3X3.
73. Stewart JJ (1990) MOPAC: a semiempirical molecular orbital program. J Comput Aided Mol Des 4:1–105
74. Cornell WD, Cieplak P, Bayly CI, Gould IR, Merz KM, Ferguson DM, Spellmeyer DC, Fox T, Caldwell JW, Kollman PA (1995) A second generation force field for the simulation of proteins, nucleic acids, and organic molecules. J Am Chem Soc 117:5179–5197
75. Halgren TA (1996) Merck molecular force field. I. Basis, form, scope, parameterization, and performance of MMFF94. J Comput Chem 17:490–519
76. Halgren TA (1996) Merck molecular force field. II. MMFF94 van der Waals and electrostatic parameters for intermolecular interactions. J Comput Chem 17:520–552
77. Halgren TA (1996) Merck molecular force field. III. Molecular geometries and vibrational frequencies for MMFF94. J Comput Chem 17:553–586
78. Halgren TA (1996) Merck molecular force field. IV. Conformational energies and geometries for MMFF94. J Comput Chem 17:587–615
79. Halgren TA, Nachbar R (1996) Merck molecular force field. V. Extension of MMFF94 using experimental data, additional computational data, and empirical rules. J Comput Chem 17:616–641
80. Halgren TA (1999) MMFF VI. MMFF94s option for energy minimization studies. J Comput Chem 20:720–729
81. Halgren TA (1999) MMFF VII. Characterization of MMFF94, MMFF94s, and other widely available force fields for conformational energies and for intermolecular-interaction energies and geometries. J Comput Chem 20:730–748
82. Sundukova M, Vilotti S, Abbate R, Fabbretti E, Nistri A (2012) Functional differences between ATP-gated human and rat P2X3 receptors are caused by critical residues of the intracellular C-terminal domain. J Neurochem 122:557–567